Low-frequency Oscillation Damping Control for Large-scale Power System with Simplified Virtual Synchronous Machine

Karim Sebaa, Yang Zhou, Yong Li, *Senior Member*, *IEEE*, Ayetül Gelen, and Hassan Nouri, *Senior Member*, *IEEE*

***Abstract*—This study focuses on a virtual synchronous machine (VSM) based on voltage source converters to mimic the behavior of synchronous machines (SMs) and improve the damping ratio of the power system. The VSM model is simplified according to some assumptions (neglecting the speed variation and the stator transients) to allow for the possibility of dealing with low-frequency oscillation in large-scale systems with many VSMs. Furthermore, a virtual power system stabilizer (VPSS) structure is proposed and tuned using a method based on a linearized power system dynamic model. The linear and nonlinear analyses examine the stability of two modified versions of a 16-machine power system in which, in the first case, partial classical machines are replaced by VSMs, and in the second case, all SMs are replaced by VSMs. The simulation results of the case studies validate the efficiency of the proposed control strategy.**

***Index Terms*—Synchronous machine (SM), small-signal stability, transient stability, virtual power system stabilizer (VPSS), virtual synchronous machine (VSM).**

NOMENCLATURE

A. Operators

Δ	Perturbation-variation operator
p	Differential operator d/dt
s	Laplace operator
$\circ$	Equilibrium script
$^{\mathrm{T}}$	Transposition script

B. Variables

δ	Angular position of rotor with respect to synchronous rotating frame
ω, ω_s	Angular speed and synchronous speed
$\boldsymbol{\psi}_{abc}=[\psi_a, \psi_b, \psi_c]^{\mathrm{T}}$	Vector of abc instantaneous stator flux
$\boldsymbol{\psi}_{dq0}=[\psi_d, \psi_q, \psi_0]^{\mathrm{T}}$	Vector of $dq0$ instantaneous stator flux
ζ	Damping ratio
$1/K$	Integrator gain
$\boldsymbol{A}$, $\boldsymbol{B}$, $\boldsymbol{C}$, and $\boldsymbol{D}$	Matrices of state, input, output, and feedforward
E_q	Synchronous internal voltage mimicked by virtual synchronous machine (VSM)
E_B	Infinite bus voltage
$\boldsymbol{e}_{abc}=[e_a, e_b, e_c]^{\mathrm{T}}$	Vector of abc instantaneous stator voltage
$\boldsymbol{e}_{dq0}=[e_d, e_q, e_0]^{\mathrm{T}}$	Vector of $dq0$ instantaneous stator voltage
e_{fd}, i_{fd}, R_{fd}, ψ_{fd}	Field voltage, current, resistance, and flux
H, D_p	Inertia constant and damping constant
K_A, T_A	Time constant and gain of automatic voltage regulator (AVR)
K_{VPSS}	Gain of virtue power system stabilizer (VPSS)
$\boldsymbol{i}_{abc}=[i_a, i_b, i_c]^{\mathrm{T}}$	Vector of abc instantaneous stator current
$\boldsymbol{i}_{dq0}=[i_d, i_q, i_0]^{\mathrm{T}}$	Vector of $dq0$ instantaneous stator current
L_{aa0}, L_{ab0}	Proper and mutual inductances of stator
$\boldsymbol{L}_{abc}$	Matrix of abc stator inductance
$\boldsymbol{L}_{abc\text{-}r}(\theta)$	Vector of abc stator-rotor mutual inductance
L_{ad}, L_{aq}	d- and q-axis mutual inductances owing to flux that links rotor circuits
$\boldsymbol{L}_{dq0}$	Matrix of $dq0$ stator inductance
$\boldsymbol{L}_{dq0\text{-}r}(\theta)$, $\boldsymbol{L}_{r\text{-}dq0}(\theta)$	Vectors of $dq0$ stator-rotor and rotor-stator mutual inductance
L_d, L_q	d- and q-axis stator self-inductances
L_{ffd}, L_{afd}	Proper inductance of field circuit and mutual inductance of stator-field circuit
L_l	Leakage inductance owing to flux that does not link any rotor circuit
$\boldsymbol{P}_\theta$	Park transformation matrix from abc variables to $dq0$ variables that keeps the same

Manuscript received: May 27, 2020; accepted: December 7, 2020. Date of CrossCheck: December 7, 2020. Date of online publication: May 17, 2021.

K. Sebaa is with the Advanced Electronics Systems Laboratory, University of Medea, Medea 26000, Algeria (e-mail: sebaa.karim@univ-medea.dz).

Y. Zhou (corresponding author) is with the Institute of Energy Systems, Energy Efficiency and Energy Economics, TU Dortmund University, Dortmund 44227, Germany (e-mail: yang.zhou@tu-dortmund.de).

Y. Li is with the College of Electrical and Information Engineering, Hunan University, Changsha 410082, China (e-mail: yongli@hnu.edu.cn).

A. Gelen is with the Department of Electrical Electronic Engineering, Bursa Technical University, Bursa 16310, Turkey (e-mail: ayetul.gelen@btu.edu.tr).

H. Nouri is with the Power Systems and Energy Research Laboratory, University of the West of England, Bristol BS16 1QY, UK (e-mail: hassan.nouri@uwe.ac.uk).

DOI: 10.35833/MPCE.2020.000340

	peak values ($\theta = \delta - \pi/2$)
P_e, Q_e	Active and reactive power outputs of VSM
P_{ref}, Q_{ref}	Reference values of active and reactive power of VSM
R_E+jX_E	Line impedance
T_e, T_m	Electrical and mechanical torques of VSM
T_w	Washout circuit time constant of VPSS
T_1, T_2, T_3, T_4	Lead-lag time constants of VPSS
T_5	Linearization time constant
$\boldsymbol{U}$, $\boldsymbol{X}$, $\boldsymbol{Y}$	Input, state space, and output variables
u_{VPSS}	Output signal of VPSS
u_{AVR}	Output signal of AVR
V_t, I_t	Terminal voltage and current of VSM
V_{ref}	Terminal reference voltage of VSM
X_s	Synchronous reactance

I. Introduction

NOWADAYS, power systems may contain many green distributed generators (DGs) supplying the power via voltage source converters (VSCs). In addition, DGs are characterized by their intermittent fluctuations and unpredictable behaviors, which might affect the overall system damping by decreasing the overall inertia [1] since they lack a rotating mass. Due to the strong electromechanical coupling in the synchronous machine (SM), the kinetic energy of the storage systems provides an additional rotating inertia, which is important for the power system stability [2], [3].

In the past, power systems possessed a sufficient inertia to dampen any eventual perturbation, and the occurrence probability of variation was small. However, this fact is no longer valid today, especially when the penetration of green sources is emerging. Accordingly, the dynamic is faster than before, and it also brings new challenges to power system control. Moreover, the oscillation becomes significant with the replacement of traditional SMs, which are the origins of rotating inertia. Hence, the damped low-frequency modes are likely to be poorer than those of the traditional power system. Some power utilities choose to limit the penetration threshold of DGs to control this growing situation [4]. However, this option is no longer a suitable choice because of the energy transition.

Since most DGs are equipped with VSCs, the missed inertia can be mimicked by an adequate pulse width modulation (PWM) strategy. The VSC that emulates SM behavior is called virtual synchronous machine (VSM) [5], [6] or sometimes synchro-inverter [7]-[9]. Many studies have explored the concept of real-time implementation of VSMs [7], [10]-[12] and how to dampen the oscillation [6], [13]-[16]. Some scholars use the supplementary control while others use the tuning of VSM parameters to emulate the power system stabilizer (PSS) and the inertia constant or damping coefficient [17], [18].

For instance, [17] tunes the parameters of the swing equation of VSM in real time by proposing the alternating moment of inertia (AMI) method, where the inertia of VSM is set to be a high value when the VSM is in the acceleration mode; otherwise, the inertia is set to be a low value when the VSM is decelerating. The only weakness of this approach is its relatively large overshooting. Recently, [18] demonstrates the direct connection of the auxiliary damping controller (ADC) to the active power loop. This is contrary to the PSS, as it is difficult to change the mechanical torque. In this approach, the system does not require any phase compensation, and pure damping can be achieved with a washout block and gain, which is directly added to the active power loop.

VSM has all the benefits and weaknesses of the SM. For example, the problem of oscillation in the SM may even exist in the VSM. VSMs exhibit oscillation as they emulate the swing equation of the classical SM. Furthermore, the option of the VSM can be extended to the PSS, which is called virtual PSS (VPSS) in this paper.

The VPSS, which has the same structure as the PSS, is implemented in the VSM routine to dampen the low-frequency oscillation. The difference between the normal PSS and VPSS should be examined. In the PSS, a supplementary signal must be added to the reference voltage of the excitation circuit; however, in the VPSS, a supplementary signal must be added to the reference voltage of the voltage-reactive power loop. Section II-C is dedicated to confirming the feasibility of such damping control through a single VSM connected to an infinite bus (SVSMIB) system. The VPSS performs better than the ADC [18], and Section II-D confirms that it can fulfill all possible control techniques and structures that the well-known PSS can achieve. Furthermore, the VPSS generates less overshooting than the AMI method. Since the performances of VPSS and ADC for the dynamic stability improvement are similar, VPSS can be considered as an alternative to the ADC.

The VSM and VPSS models are added to the power system toolbox (PST) [19] for a time-domain simulation and linear routine platform. VPSS tuning follows the classical approach proposed by Larsen [20], where the VPSS provides a phase lag between the reference and output voltages of VSM as small as possible.

The most suitable domain for studying electromechanical oscillation is the phasor domain. Hence, a PSS-VSM phasor model is used to analyze the dynamic stability of large-scale power systems with many VSMs, where the coordination of the damping controllers, namely VPSSs, is required because the control of one oscillation mode can alter the other modes. By adopting some assumptions in the phasor model discussed in Section II, the simulation step size can be increased, helping increase the system size and simulation time. This is how well-known commercial packages such as Eurostag®, PowerFactory®, and PSS/E® simulate large-scale systems in the phasor model for system-wide stability studies for a simulation period varying from a few seconds to 10-20 min.

The main contributions of this study are as follows.

1) The phasor models of the VSM and PSS-VSM are derived and established. The VSM model is simplified to im-

prove the efficiency so that it can handle the stability problem of large-scale power systems containing many VSMs.

2) Based on the phasor models, the VPSS controller is proposed to dampen the oscillation by adding a supplementary signal to the reference voltage of the voltage-reactive power loop.

3) A classical adjustment method is applied to complete the coordinated control of multiple VPSS damping controllers.

Therefore, the main focus of this study is to acquire the knowledge of the system behavior when it contains many VSMs and investigate how the VPSS dampens the power system oscillation. To investigate the occurrence of low-frequency modes and the ability of the VSMs to improve the power system inertia, a modified IEEE 68-bus New York-New England power system is used as the benchmark where some SMs are replaced by VSMs.

Furthermore, the tuning of VPSS parameters uses the classical tuning method in conjunction with the modal analysis and the participation factors to identify which part of the network is responsible for the oscillation and at which VSM the VPSS should be installed.

II. Control Strategy Analysis

Since the VSM mimics the SM behavior, it is appropriate to follow the procedures used for the classic SM model. Many different SM models in the literature are based on the current orientation, operation mode (motor or generator), and assumptions [2], [19]. However, considering that the VSC has to imitate the SM behavior, Kundur's approach [2] is most suitable for this purpose.

The VSM model is simplified in this study with some assumptions, which are divided into two parts as follows.

1) The first part is related to the choice made on the VSM structure, such as neglecting the eddy currents, damper effects, saturation, and unbalanced operation. These assumptions were adopted by [7].

2) The second part is mandatory to study the electromechanical oscillation where the phasor domain is selected and the PST package is used, which consists of neglecting the transformer voltage terms, neglecting the effect of speed variation, and finally neglecting the saliency, as the PST package assumes no saliency. These assumptions lead to a significant reduction in the computation time and allow us to increase the integration steps for the simulation of a large-scale power system.

Assuming that the rotor is round and the stator has a small resistance, which can be neglected, the stator and rotor voltages are shown as (1) and (2), respectively.

$$\boldsymbol{e}_{abc}=\mathrm{p}\boldsymbol{\psi}_{abc} \tag{1}$$

$$e_{fd}=R_{fd}i_{fd}+\mathrm{p}\psi_{fd} \tag{2}$$

With neglecting the saturation, the flux is linearly dependent on the current, which is expressed as:

$$\begin{bmatrix}\boldsymbol{\psi}_{abc}\\ \psi_{fd}\end{bmatrix}=\begin{bmatrix}\boldsymbol{L}_{abc} & \boldsymbol{L}_{abc\text{-}r}(\theta)\\ \boldsymbol{L}_{abc\text{-}r}(\theta)^{\mathrm{T}} & L_{ffd}\end{bmatrix}\begin{bmatrix}\boldsymbol{i}_{abc}\\ i_{fd}\end{bmatrix} \tag{3}$$

The inductance matrices can be defined as:

$$\begin{cases}\boldsymbol{L}_{abc}=\begin{bmatrix}-L_{aa0} & L_{ab0} & L_{ab0}\\ L_{ab0} & -L_{aa0} & L_{ab0}\\ L_{ab0} & L_{ab0} & -L_{aa0}\end{bmatrix}\\ \boldsymbol{L}_{\mathrm{abc}\text{-}r}=L_{afd}\left[\cos\theta \quad \cos\left(\theta-\dfrac{2\pi}{3}\right) \quad \cos\left(\theta+\dfrac{2\pi}{3}\right)\right]^{\mathrm{T}}\end{cases} \tag{4}$$

Using the Park transformation matrix $\boldsymbol{P}_{\theta}$ that keeps the same peak values, it is easy to obtain:

$$\begin{bmatrix}\boldsymbol{\psi}_{dq0}\\ \psi_{fd}\end{bmatrix}=\begin{bmatrix}-\boldsymbol{L}_{dq0} & \boldsymbol{L}_{dq0\text{-}r}\\ \boldsymbol{L}_{r\text{-}dq0} & -L_{ffd}\end{bmatrix}\begin{bmatrix}\boldsymbol{i}_{dq0}\\ i_{fd}\end{bmatrix} \tag{5}$$

The previous matrix is created as:

$$\begin{cases}\boldsymbol{L}_{dq0}=\mathrm{diag}(L_d,L_q,L_0)\\ \boldsymbol{L}_{dq0\text{-}r}=\begin{bmatrix}L_{afd} & 0 & 0\end{bmatrix}^{\mathrm{T}}\\ L_0=0\\ \boldsymbol{L}_{r\text{-}dq0}=\begin{bmatrix}-\dfrac{3}{2}L_{afd} & 0 & 0\end{bmatrix}\\ L_d=L_q=L_{aa0}+L_{ab0}\\ \boldsymbol{e}_{dq0}=\omega\begin{bmatrix}0 & -1 & 0\\ 1 & 0 & 0\\ 0 & 0 & 0\end{bmatrix}\boldsymbol{\psi}_{dq0}+\mathrm{p}\boldsymbol{\psi}_{dq0}\end{cases} \tag{6}$$

The speed voltages $\psi_q\mathrm{p}\theta$ and $\psi_d\mathrm{p}\theta$ are sufficiently slow-varying so that they are considered as constant. However, the transformer voltage terms $\mathrm{p}\boldsymbol{\psi}_{dq0}$ are usually neglected because the stator transients are sufficiently fast that it is not recommended to be considered. Based on assumptions, we can obtain:

$$\begin{cases}e_d=-\omega\psi_q=\omega L_q i_q\\ e_q=\omega\psi_d=-\omega L_d i_d+\omega L_{afd}i_{fd}\\ e_{fd}=R_{fd}i_d+\mathrm{p}\left(L_{ffd}i_{fd}-\dfrac{3}{2}L_{afd}i_d\right)\end{cases} \tag{7}$$

The per-unit transformation is based on the guidelines outlined in [2], and the leakage inductance L_l and mutual inductance L_{ad} are decomposed as:

$$\begin{cases}e_d=\omega(L_l+L_{aq})i_q\\ e_q=-\omega(L_l+L_{ad})i_d+\omega L_{ad}i_{fd}\\ e_{fd}=R_{fd}i_d+\mathrm{p}(L_{ffd}i_{fd}-L_{ad}i_d)\end{cases} \tag{8}$$

As the angular speed is assumed to change very slowly, we take it as a constant, namely $\omega\approx 1$ p.u.. By neglecting saliency, $X_s=L_l+L_{ad}=L_l+L_{aq}$, which allows us to develop the simplified phasor representation of the VSM as:

$$e_d=X_s i_q \tag{9}$$

$$e_q=-X_s i_d+\omega L_{ad}i_{fd}=-X_s i_d+E_q \tag{10}$$

where $E_q=\omega L_{ad}i_{fd}$.

The active and reactive power sent to the network can be calculated by:

$$P_e=e_d i_d+e_q i_q=\omega L_{ad}i_{fd}i_q \tag{11}$$

$$Q_e=-e_d i_q+e_q i_d=\omega L_{ad}i_{fd}i_d-X_s(i_d^2+i_q^2) \tag{12}$$

The term $L_{ad}i_{fd}$ in (8) - (10) is the control variable that

matches the SM behavior.

The mechanical part of the SM is vital for damping power system oscillation. Based on Newton's first law, the per-unit swing equation is:

$$\mathrm{p}\omega = \frac{1}{2H}\left[P_{ref} - P_e - D_p(\omega - 1)\right] \tag{13}$$

$$\mathrm{p}\delta = \omega_s(\omega - 1) \tag{14}$$

The structures of the active power, reactive power, and voltage regulation of the VSM taken from [7], which are improved by the automatic voltage regulator (AVR) and the VPSS, are shown in Fig. 1. As the terminal voltage V_t is close to E_q ($V_t \approx E_q$), E_q can replace V_t for the AVR input. The fictive reactance X_s of the VSM is assumed to belong to the network. The stator resistance r_s can be added, but here it is neglected.

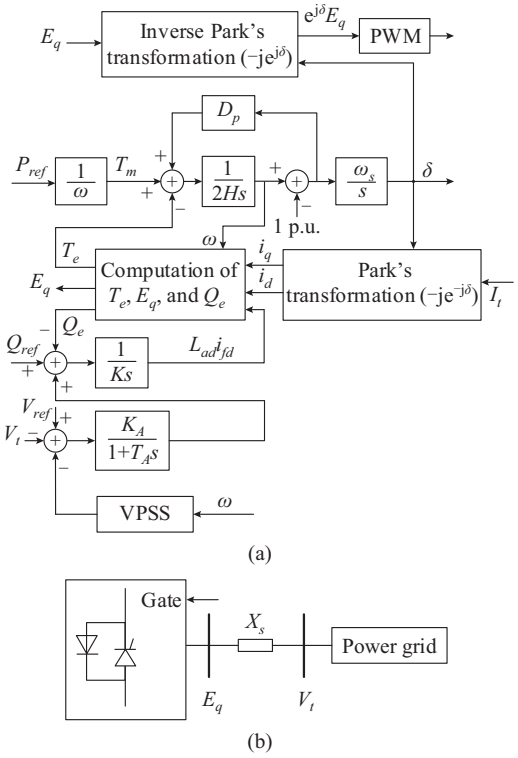

Fig. 1. Schematic diagram of VSM. (a) Structure of VSM. (b) VSM connecting to power grid.

The load flow is performed to initialize the state variables of the VSM and obtain the reference values of active and reactive power P_{ref} and Q_{ref} and the terminal voltage reference V_{ref}. The basic state variables of VSM are $\omega, \delta, L_{ad}i_{fd}$ and they can be augmented by the state variables of the AVR and VPSS.

The three basic state variables are initialized as:

$$\omega(0) = 1 \tag{15}$$

$$\delta(0) = \arctan(V_t + \mathrm{j}X_s I_t) \tag{16}$$

$$L_{ad}i_{fd}(0) = \frac{P}{\mathrm{Im}\left(I_t e^{\mathrm{j}\left(\frac{\pi}{2} - \delta(0)\right)}\right)} \tag{17}$$

A. VPSS Control Method

The VPSS is a controller that acts as a classical PSS by adding an auxiliary signal to dampen the power swing rapidly and improve the power system dynamic performance. Its structure is summarized by the following transfer function:

$$u_{VPSS} = K_{VPSS}\frac{sT_w}{1+sT_w}\frac{1+sT_1}{1+sT_2}\frac{1+sT_3}{1+sT_4}\Delta\omega \tag{18}$$

The speed variation signal is selected from the commonly used signal to this end. The VPSS can sense the power change of the VSM, control the reference value of reactive power, and dampen the oscillation by producing an adequate component of the electrical power of VSM in phase with the speed change. The VSM should guarantee an adequate phase compensation block for the phase lag between V_{ref} and P_e [20].

B. Accuracy of Approximate Model

As mentioned in Section II-A, the assumptions are grouped into two parts. The first part is related to the choice made on the SM to be imitated (or SM imitation). In the second part, the transformer voltage term $\mathrm{p}\boldsymbol{\psi}_{dq0}$ and the effect of the speed variation are neglected, as the interest of our study is in the power system stability.

The terms $\mathrm{p}\psi_q$ and $\mathrm{p}\psi_d$ represent the stator transient (i.e., the AC side of the VSC). By neglecting these terms, we keep only the fundamental frequency components, which causes the stator voltage equations to appear as algebraic ones. This approach is justified by the fact that the transient associated with the network decays quickly. Hence, it is almost unnecessary to model the effects of these terms. Moreover, to counterbalance the effect of neglecting these terms, the effect of the speed variation in the stator is neglected [2].

To confirm these assumptions, a three-phase short-circuit fault with duration is applied during the six cycles on an SVSMIB system shown in Fig. 2 (the SVSMIB parameters are presented in Appendix A) and cleared within 0.1.

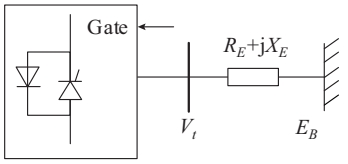

Fig. 2. Schematic diagram of SVSMIB system.

Figure 3 shows the response of the system with and without the two aforementioned assumptions (neglecting or including the transformer voltages $\mathrm{p}\psi_q, \mathrm{p}\psi_d$ and speed variation), which confirms that it is an acceptable assumption to omit the transformer voltage and speed variation terms. The inclusion of these transients significantly increases the order of the overall system; hence, it limits the system size to be simulated. Furthermore, the system without these assumptions requires a small time step, as it contains high-frequency components, which dramatically increases the computation costs.

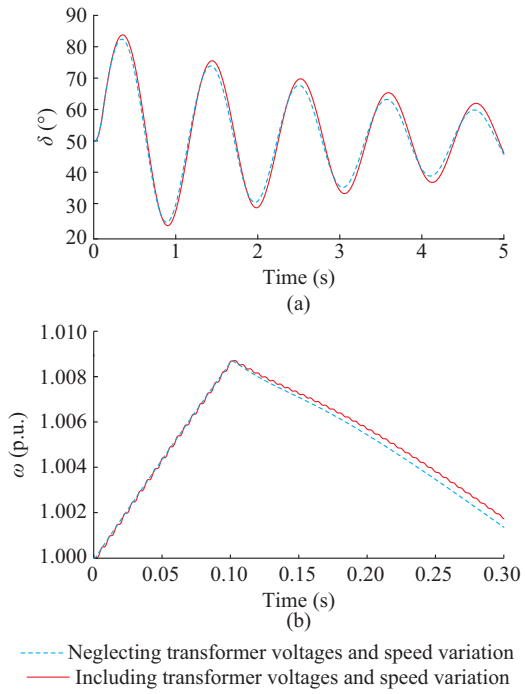

Fig. 3. Effect of neglecting or including transformer voltages and speed variation. (a) Response profile of rotor angle δ. (b) Response profile of generator speed ω.

C. Small-signal Analysis for SVSMIB

To examine the ability of the proposed VPSS to produce a damping torque component (i.e., a component in phase with the deviation of angular speed), the small-signal model of the SVSMIB system shown in Fig. 2 is developed.

Around an equilibrium operation point (δ^0, E_q^0, V_t^0), the system is perturbed to obtain the following linearized equations:

$$\begin{cases} \Delta i_d = m_1 \Delta\delta + m_2 \Delta E_q \\ \Delta i_q = n_1 \Delta\delta + n_2 \Delta E_q \\ \Delta T_e = K_1 \Delta\delta + K_2 \Delta E_q \\ \Delta Q_e = K_3 \Delta\delta + K_4 \Delta E_q \\ \Delta V_t = K_6 \Delta\delta + K_7 \Delta E_q \end{cases} \tag{19}$$

Appendix A presents the constants K_1 - K_7 and other parameters (m_1, m_2, n_1, n_2) related to the system in Fig. 2. Figure 4 depicts the linearized system after adding the swing equation and virtual AVR.

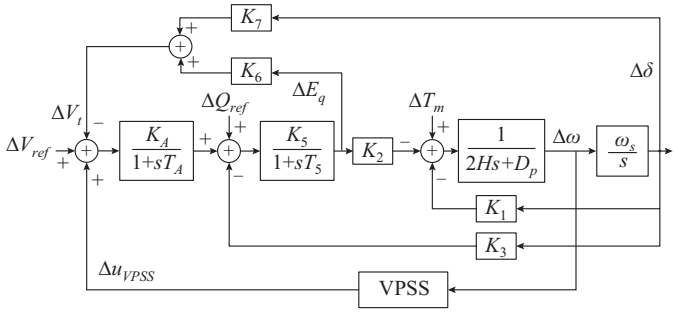

Fig. 4. Diagram of linearized SVSMIB system.

Assuming a low time constant T_A (i.e., $T_A \approx 0$), ΔE_q produced by the VPSS is given by:

$$\Delta E_q = \frac{K_5 K_A}{1+sT_5}(-K_7 \Delta E_q + \Delta u_{VPSS}) \tag{20}$$

By grouping the ΔE_q terms and rearranging, we can obtain:

$$\frac{\Delta E_q}{\Delta u_{VPSS}} = \frac{K_5 K_A}{sT_5 + 1 + K_5 K_7 K_A} = \frac{11.61}{2.32s + 8.71} \tag{21}$$

The torque ΔT_{VPSS} provided by the VPSS is calculated as:

$$\frac{\Delta T_{VPSS}}{\Delta u_{VPSS}} = \frac{K_2 \Delta E_q}{\Delta u_{VPSS}} = \frac{9.30}{1.39s + 8.71} \tag{22}$$

This system exhibits only one local mode, typically with a frequency of 1 Hz ($s = 6$j, $f = 1$ Hz). Hence, at $s = 6$j, (22) gives $\Delta T_{VPSS} = (1.05\angle -9°)\Delta u_{VPSS}$. For a pure damping torque, ΔT_{VPSS} should be in phase with $\Delta\omega$ at a frequency of 1 Hz, and $\Delta\omega$ should be proceeded via a phase-lead compensator (i.e., VPSS) so that the signal is advanced by 9° at 1 Hz. The appropriate phase-lead network is in cascade with a washout block that serves to subtract the low-frequency components of the signal. The gain $K_{VPSS} = 10$ is obtained from the root-locus plot (as shown in Fig. 5), which provides sufficient damping (15%). Hence, the adequate lead lag VPSS can be calculated as:

$$\Delta u = K_{VPSS}\left(\frac{10s}{1+10s}\right)\left(\frac{1+0.19s}{1+0.14s}\right)\Delta\omega \tag{23}$$

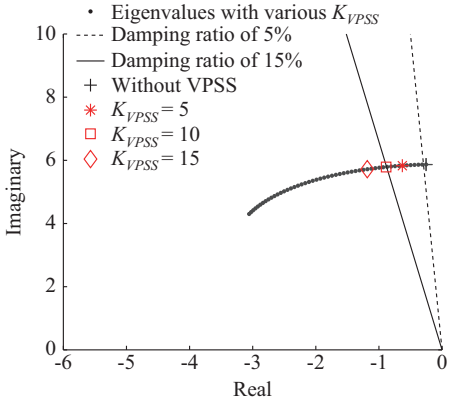

Fig. 5. Eigenvalues with VPSS gain.

The speed deviation owing to a 1% increase in ΔT_m at 1 s is presented in Fig. 6, which indicates that the VPSS is an option to enhance the system damping.

For comparison, the control methods of [17], [18] are selected. For example, as discussed earlier, the AMI method in [17] sets a large value of the inertia to $H_{big} = H$ and a small value to $H_{small} = H/6$, which is known as the bang-bang control strategy. However, [18] uses the concept of accessibility to the power reference control (unlike the SM, where the access to the mechanical torque control is difficult), where the ADC consists of a gain, a washout, and the phase compensation, i.e., $ADC(s) = 100s(1+0.19s)/[(1+10s)(1+0.14s)]$. Note that the phase to be compensated is $P_e(s)/P_{ref}(s)$.

It is important to underline that we can use the ADC without its phase compensation, just with its gain and its washout block ($100s/(1+10s)$), as it will act directly as an ideal damper.

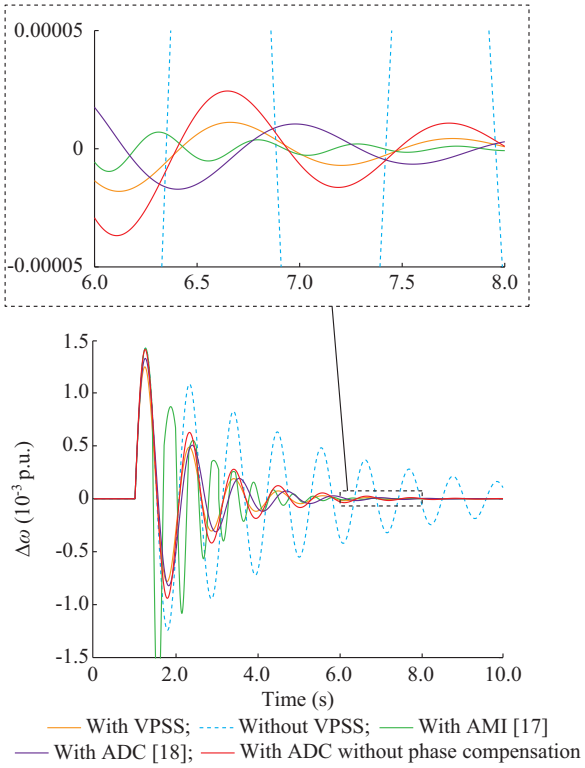

Fig. 6. Comparison of proposed VPSS with different control methods.

Figure 6 clearly shows that the AMI method is characterized by a relatively high overshooting among the three methods, i.e., the proposed VPSS, AMI method, and ADC. However, the performance and control design processes of both methods, i. e., the proposed VPSS and ADC, are similar. Hence, VPSS can be considered as a new alternative to the ADC. Furthermore, a closer inspection of the enlarged view in Fig. 6 suggests that the VPSS can stabilize the system slightly faster than the ADC.

D. Small-signal Analysis for Multimachine System

Before the small-signal analysis, the state space model of a power system with one or more machines should be built around an equilibrium point (operation point):

$$\begin{cases} \mathrm{p}\boldsymbol{X} = \boldsymbol{AX} + \boldsymbol{BU} \\ \boldsymbol{Y} = \boldsymbol{CX} + \boldsymbol{DU} \end{cases} \tag{24}$$

This linearized model can be constructed in two ways. The first is the analytical method in which the linearized models of each device are computed analytically from the Jacobian matrices of the nonlinear state equations of the devices, and all individual state space models are gathered with the algebraic equations representing the network and the stators of machines to build the full linearized model depicted in (24) [20].

Although the analytical method is accurate, the models for the nonlinear simulation are different from those for the linear analysis. On the other hand, the numerical method is an alternative, where the Jacobian matrix is calculated numerically using a sequence of small perturbations for each state variable, even though it is less accurate than the analytical method. However, it has the advantage that the models used for the linear and nonlinear simulations are the same.

In this study, the PST is used, where the linearized model is computed numerically. To increase the accuracy of the numerical method, the perturbation is performed for negative as well as positive steps, and the average values are taken [21]. Furthermore, newly emerging techniques can be selected, which are semianalytical methods, using the power series in the time domain to approximate the differential-algebraic equations of the power system [22].

III. Case Study

A. System Description

The most commonly used power system in low-frequency studies is the multimachine power system [20], as depicted in Fig. 7. This network contains five areas. Area 5 and practically the entire area 4 have detailed models. However, each of the remaining areas (areas 1, 2, and 3) is represented by one equivalent machine.

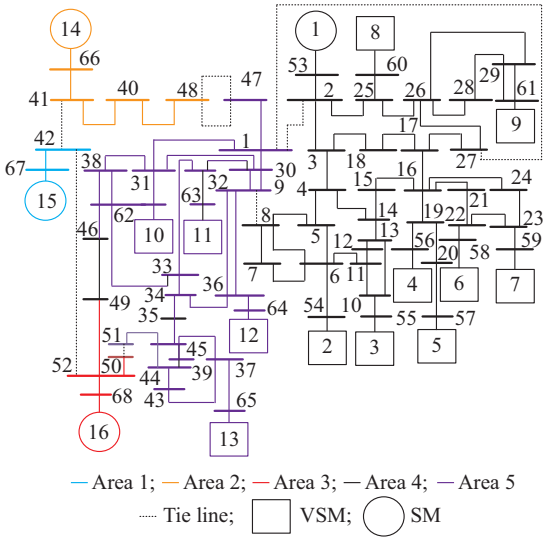

Fig. 7. Modified IEEE 68-bus New York-New England power system with VSMs in areas 4 and 5 (case 1).

To examine the ability of the virtual synchronous generators to dampen the low-frequency oscillation, three cases are analyzed.

Case 1: only the classical SMs in areas 4 and 5 are replaced by identical VSMs (except for generator 1).

Case 2: all the 16 classical SMs are replaced by identical VSMs.

Case 3: all the 16 classical SMs are kept in service [19].

The VSM parameters are summarized in Table I, the data of which are taken from [20], ensuring that the behavior of the VSM is closer to that of classical SMs. For the VPSS parameters, T_1 - T_4 are chosen to provide a phase lead in the frequency range of 0.1-2 Hz. The gain K_{VPSS} is chosen to provide adequate damping and should be minimized as much as possible. T_w is selected from 1-20 s. K_A and T_A represent the simple virtual AVR constants. H and X_s are taken to be equal to the SM values they replace. From Fig. 1, the time

constant of the frequency-droop loop is $\tau_f = 2H/D_p$ [7]. If we adopt $\tau_f = 0.01$ s, then $D_p = 2H$ because the delay is neglected, and τ_f can be quite small. Similarly, $\tau_v = K/(\omega_s K_A)$ (if T_A is neglected). If K_A and τ_v have already been fixed, K can be easily set. The abovementioned time constants can be set to be very small values because no delay is involved in these two loops, unlike the case of the SM where delays exist.

TABLE I
VSM PARAMETERS

Symbol	Value
H(s)	3.4000; 4.9494; 4.9623; 4.1629 4.7667; 4.9107; 4.3267; 3.9150 4.0365; 2.9106; 2.0053; 5.1791 4.0782; 3.0000; 3.0000; 4.4500
D_p	0.6800; 0.9899; 0.9925; 0.8326 0.9533; 0.9821; 0.8653; 0.7830 0.8073; 0.5821; 0.4011; 1.0358 0.8156; 0.6000; 0.6000; 0.8900
K	3.77
T_A(s)	0.01
K_A	1
X_s	0.2480; 0.4253; 0.3831; 0.2995 0.3600; 0.3543; 0.2990; 0.3538 0.4872; 0.4868; 0.2531; 0.5525 0.3345; 0.2850; 0.2850; 0.3590

B. Small-signal Stability Analysis Results

The linear analysis of the power system for case 1 reveals many poorly-damped eigenvalues (with a damping ratio of less than 5%) and one unstable mode (at the right-half side), as shown in Fig. 8.

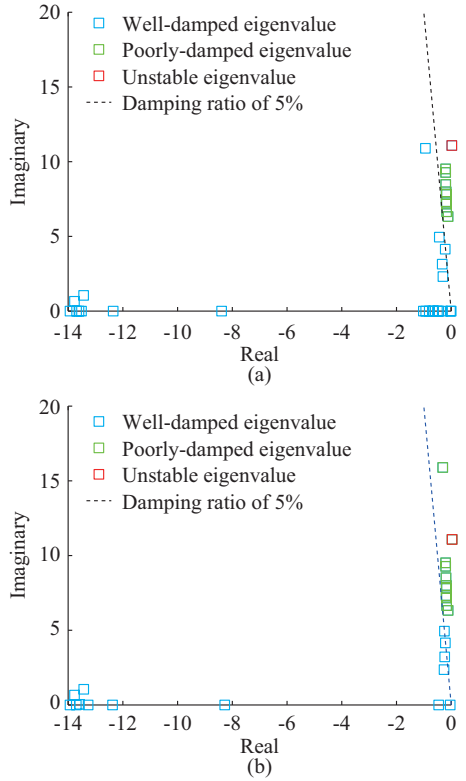

Fig. 8. Results of eigenvalues. (a) Case 1. (b) Case 2.

This network exhibits 10 oscillatory low-frequency modes in case 1 (as shown in Table II) and 12 oscillatory low-frequency modes in case 2 (as shown in Table III). In case 1, the frequency range of these modes is from 1.0070 to 1.7639 Hz. There are nine stable poorly-damped modes and one unstable mode. All of these 10 modes are local ones, as their frequencies range from 1 to 2 Hz.

TABLE II
POORLY-DAMPED MODES IN CASE 1

Mode index	Mode	f (Hz)	ζ (%)	No. of VSM
20	–0.1172 + j6.3274	1.0070	1.8519	9
22	–0.1680 + j6.6492	1.0583	2.5264	2
24	–0.1781 + j7.1645	1.1403	2.4850	12
26	–0.1859 + j7.3216	1.1653	2.5385	5
28	–0.1762 + j7.8011	1.2416	2.2578	3
30	–0.1867 + j7.9838	1.2707	2.3384	10
33	–0.2012 + j8.4734	1.3486	2.3736	8
35	–0.2027 + j9.2800	1.4770	2.1840	7
37	–0.2039 + j9.5149	1.5143	2.1429	4
41	**0.0208 + j11.0828**	**1.7639**	**–0.1879**	**11**

Note: bold mode is unstable mode.

TABLE III
POORLY-DAMPED MODES IN CASE 2

Mode index	Mode	f (Hz)	ζ (%)	No. of VSM
4	**–0.2624 + j2.3648**	**0.3764**	**0.1103**	**13, 15, 14**
12	–0.1154 + j6.3294	1.0074	1.8231	9
14	–0.1679 + j6.6502	1.0584	2.5243	2
16	–0.1778 + j7.1646	1.1403	2.4814	12
18	–0.1859 + j7.3216	1.1653	2.5389	5
20	–0.1759 + j7.8016	1.2417	2.2543	3
22	–0.1840 + j7.9979	1.2729	2.2995	10
25	–0.1922 + j8.5164	1.3554	2.2559	8
27	–0.2027 + j9.2800	1.4770	2.1840	7
29	–0.2039 + j9.5150	1.5144	2.1426	4
31	**0.0310 + j11.0794**	**1.7633**	**–0.2796**	**11**
55	–0.3103 +j15.8961	2.5299	1.9519	1

Note: underlined mode is interarea, which is presented to show characteristics of this type of mode.

The speed participation factor (SPF) can identify which VSM is responsible for the undamped mode. The SPF of the j^{th} mode for a change in the i^{th} diagonal element that corresponds to the speed state variable order is calculated as:

$$p_{ij} = v_j(i)u_j(i) \tag{25}$$

In addition, the SPF indicates which VSM speed signal could significantly impact an eventual mode. Figure 9 shows the SPFs of the low-frequency modes in case 1. The number of VSMs that participate in a mode increases when the mode frequency decreases. The modes with a higher frequency are the local ones associated with fewer machines. Conversely, those with a lower frequency are the intermodes and involve more virtual machines.

A VPSS is proposed to increase the damping ratio ζ of these modes, as shown in Fig. 1. The bar charts depict a VSM where the highest value of the real SPF coincides. These modes are associated mainly with these machines, and VPSSs at these VSMs are mandatory. Another choice con-

sists of the tuning of D_p and H. This option is examined at the end of this study. The 41st mode is owing to the oscillation of VSM 11 against the entire system. It is essential to increase the damping of this mode using a VPSS.

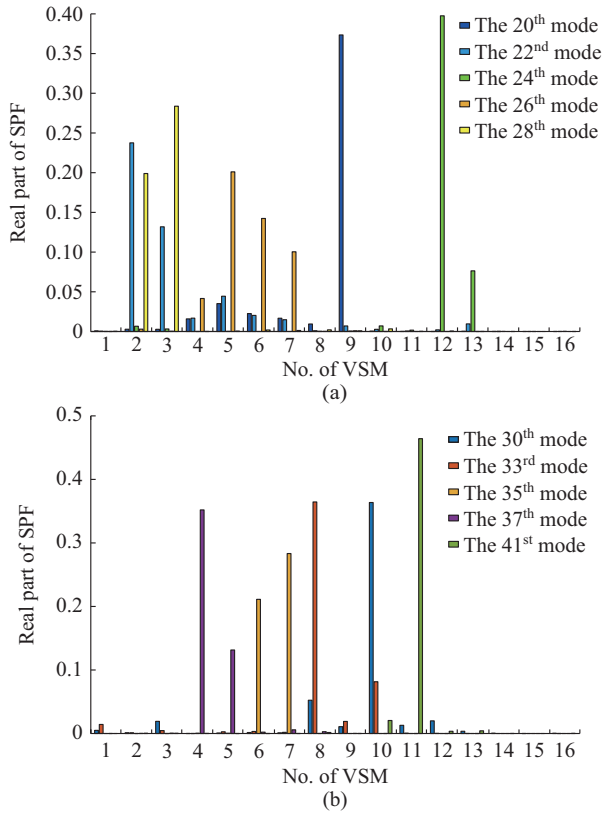

Fig. 9. SPFs of low-frequency modes in case 1. (a) The 20th, 22nd , 24th, 26th, and 28th modes. (b) The 30th, 33rd, 35th, 37th, and 41st modes.

C. VPSS Control Results

Considering that the frequency and angle do not vary, the VPSS phase lead must match the phase lag between VSM reference voltage of VSM V_{ref} and active power output of VSM P_e as much as possible. Practically, this can be achieved by eliminating the rows and columns of the state space matrices corresponding to the state variables of angle and angular speed [20]. This cannot be measured; however, this phase is close to the negative of the phase lead between V_{ref} and V_t, which could be measured in-situ with system conditions so that all modes are stable.

First, the ideal phase lead of each VSM is evaluated separately, as they are independent of the VPSS [20]. Then, we add the first VPSS and adjust its gain until we meet the desirable damping. The second VPSS is added to the system with the first VPSS, and the gain of the second VPSS is adjusted. This step-by-step method is followed until we guarantee an acceptable minimum damping ratio, generally greater than 5% [20].

The proposed VPSS phase-lead compensation elaborated by the trial error method is shown as Fig. 10 in blue. With such a phase compensator, the VPSS acts as an ideal damper, i.e., it produces a torque in antiphase to the VSM speed in the range of frequencies that are of interest (0.1-2.0 Hz). Since the VSMs have the same time constant loops, the obtained compensation works well for all of the machines.

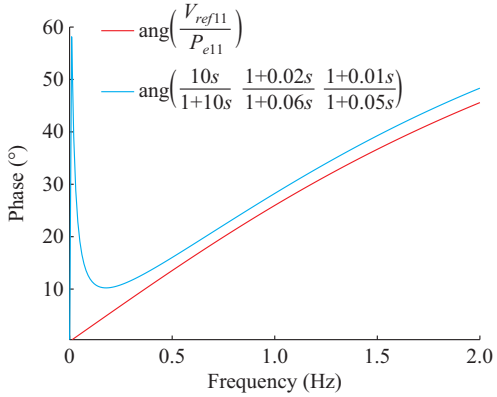

Fig. 10. Ideal PSS phase lead and proposed VPSS phase-lead compensation.

Figure 11 shows the root locus, which reveals that $K_{11}=50$ is sufficient to move away the mode of interest from the unstable area, even over the damping ratio of 10%. The gain of the compensator at high frequencies, which is proportional to T_1T_3/T_2T_4, should be minimized as much as possible. Furthermore, the damping ratio is 18.5%. As mentioned above, the 41st mode is a local one, and there are no other altered ones.

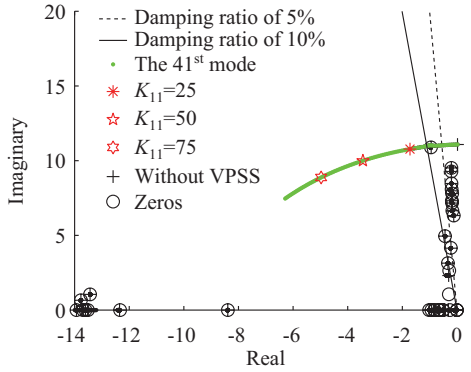

Fig. 11. Root locus with VPSS gain VSM 11.

Applying the previous method to the remaining 10 modes leads to undesirable and poorly-damped modes. In particular, these are interarea modes associated with more than one VSM. Accordingly, when the damping ratio of the local modes increases, those relative to the interarea modes may decrease. The same analysis is performed for case 2; however, the results of case 3 are taken from [19]. Table IV summarizes the VPSS gains for cases 1 and 2, which are obtained through the root-locus method. Notice that the VPSS time constants are the same for cases 1 and 2, as depicted in Fig. 10 (T_w = 10, T_1 = 0.02 s, T_2 = 0.06 s, T_3 = 0.01 s, and T_4 = 0.01 s). Figure 12 depicts the linear analysis for cases 1 and 2. The minimum damping ratio increases to 10%. Thus, the system damping becomes sufficient.

TABLE IV
VPSS GAINS

Number of VSM	Gain	
	Case 1	Case 2
1		10
2	50	70
3	40	45
4	40	70
5	50	45
7	50	70
8	40	60
9	50	70
10	40	30
11	50	30
12	50	70
14		70

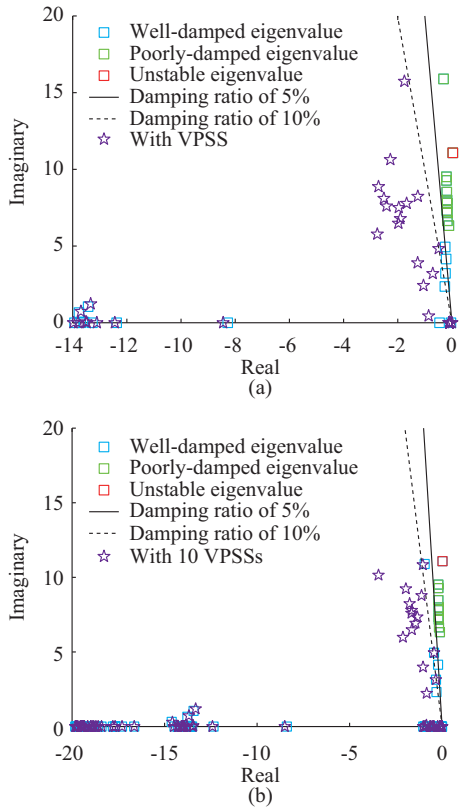

Fig. 12. Eigenvalues of 16 VSMs and 12 VPSSs. (a) Case 1. (b) Case 2.

D. VSM-VPSS Damping Performance Analysis

Two contingencies check the trustworthiness and reliability of the VSMs and VPSS for damping the low-frequency modes. In the first contingency, a three-phase fault at bus 1 on line 1-2 is applied during six cycles. In the second contingency, a three-phase fault at bus 29 on line 29-28 is applied for the same duration.

As shown in Figs. 13 and 14, it is confirmed that the VPSS increases the overall system damping. For both contingencies, the angular speeds converge to steady values faster with the VPSS.

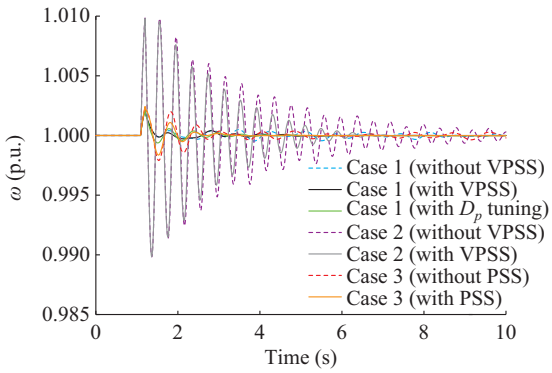

Fig. 13. Diagram of the first contingency.

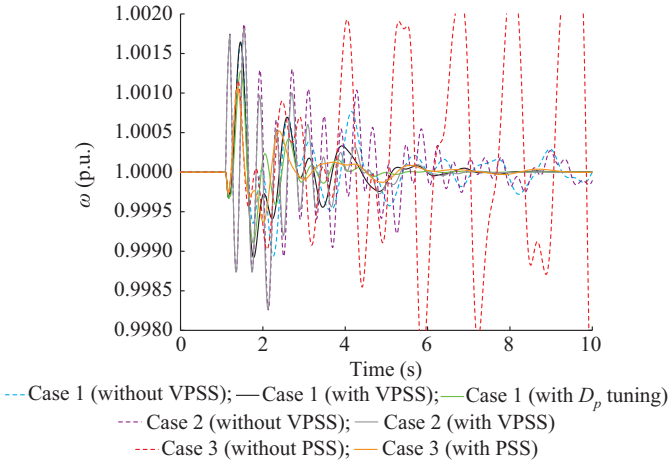

Fig. 14. Diagram of the second contingency.

E. Tuning Analysis of D_p

In this subsection, the impact of the parameter D_p on the oscillation mode damping is studied. For each value of D_p, from its initial value to a relatively infinite value ($+\infty$), the system is linearized, and the eigenvalues are computed to define the value of D_p that improves the damping of the desired mode without altering other modes.

Case 1 is taken as an example. Based on Tables II and III, the 41st mode is related to VSM 11. Consequently, D_{p11} will be varied until the damping ratio of the 41st mode exceeds 10%. Figure 15 shows the linear analysis when D_{p11} changes from its initial value to a relatively infinite value. It is adequate for the value of D_{p11} to be 15.

The same method is adopted for the remaining modes until all of them are moved to the desired damping area. The obtained new D_p values are shown in Fig. 16.

Based on the angular speed of the first SM represented in Figs. 13 and 14, it seems that both of the proposed methods can dampen the low-frequency oscillation. The angular speed of the first machine reaches its steady-state value for the two contingencies. The VPSS damping technique is preferred because it allows us to easily determine the desired damping ratio and which part of the system is responsible for the undamped mode. This can be considered as an extrinsic method. However, the D_p technique is regarded as an intrinsic method as it acts on one of the VSM parameters.

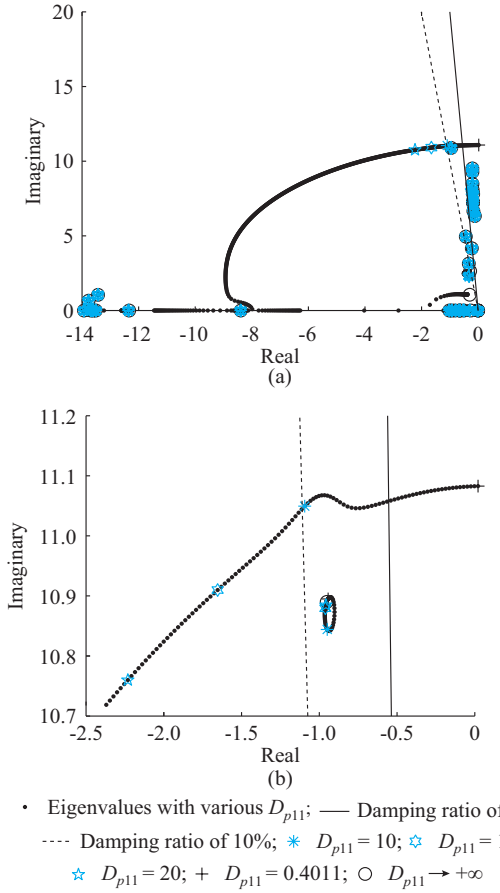

Fig. 15. Eigenvalues when D_{p11} changes from 0.4011 to $+\infty$. (a) Full plot. (b) Zoom around the 41st mode.

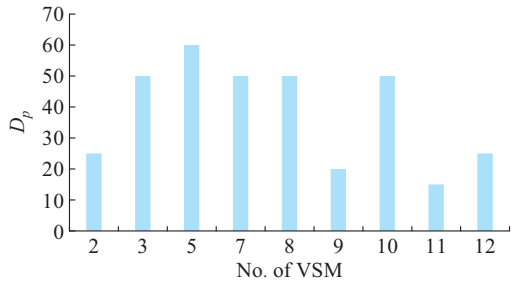

Fig. 16. Modified coefficient D_p of VPSS.

IV. Conclusion

In this paper, the VSM modeling and tuning are presented to investigate and mitigate the poorly-damped modes in current power systems with several green energy sources. Moreover, the ability of power systems to operate in presence of the inverter-based generation would be possible only by adding a damping controller such as the VPSS or by adjusting the damping constant D_p. Due to the lack of inertia, the inverter-based sources exhibit eventually undamped and/or unstable low-frequency modes. Nevertheless, the VPSS well masters damping in line with other available methods.

In this study, it was assumed that VSMs are plugged into constant-power green sources. In future work, various wind turbines and photovoltaic models will be added.

Appendix A

System algebraic and differential equations are given as:

$$\mathrm{p}\Delta\omega=\frac{1}{2H}(T_{ref}-T_e-D_p\Delta\omega) \tag{A1}$$

$$\mathrm{p}\delta=\omega_s\Delta\omega \tag{A2}$$

$$\mathrm{p}E_q=\frac{1}{K}\left(Q_{ref}-Q_e+u_{AVR}\right) \tag{A3}$$

$$\begin{cases} i_d=\dfrac{1}{R_T^2+X_T^2}\left[-R_TE_B\sin\delta+X_T\left(-E_B\cos\delta+E_q\right)\right] \\ i_q=\dfrac{1}{R_T^2+X_T^2}\left[X_TE_B\sin\delta+R_T\left(-E_B\cos\delta+E_q\right)\right] \end{cases} \tag{A4}$$

$$T_e=E_qi_q \tag{A5}$$

$$Q_e=E_qi_d-X_s\left(i_d^2+i_q^2\right) \tag{A6}$$

$$\begin{cases} R_T=R_E \\ X_T=X_E+X_s \end{cases} \tag{A7}$$

$$n_1=\frac{E_B}{R_T^2+X_T^2}\left(X_T\cos\delta^0+R_T\sin\delta^0\right) \tag{A8}$$

$$n_2=\frac{R_T}{R_T{}^2+X_T{}^2} \tag{A9}$$

$$m_1=\frac{E_B}{R_T^2+X_T^2}\left(-R_T\cos\delta^0+X_T\sin\delta^0\right) \tag{A10}$$

$$m_2=\frac{X_T}{R_T^2+X_T^2} \tag{A11}$$

$$K_1=n_1E_q^0 \tag{A12}$$

$$K_2=n_2E_q^0+i_q^0 \tag{A13}$$

$$K_3=m_1\left(E_q^0-2X_si_d^0\right)-2n_1X_si_q^0 \tag{A14}$$

$$K_4=m_2\left(E_q^0-2X_si_d^0\right)-2n_2X_si_q^0 \tag{A15}$$

$$K_5=\frac{1}{K_4} \tag{A16}$$

$$T_5=K/K_4 \tag{A17}$$

$$K_6=\left(n_1X_se_d^0-m_1X_se_q^0\right)/V_t^0 \tag{A18}$$

$$K_7=\left[n_2X_se_d^0-\left(m_2X_s+1\right)e_q^0\right]/V_t^0 \tag{A19}$$

SVSMIB parameters are given as shown in Table AI.

TABLE AI
SVSMIB Parameters

Parameter	Value	Parameter	Value
P_e	0.9 p.u.	X_E	0.65 p.u.
Q_e	0.3 p.u.	H	5 s
V_t	1∠36° p.u.	D_p	6 p.u.
E_B	0.995 p.u.	K	0.2
X_s	0.3 p.u.	K_A	10
R_E	0 p.u.	T_A	0 s

SVSMIB initial values are calculated as shown in Table AII.

TABLE AII
SVSMIB INITIAL VALUES

Variable	Initial value
δ^0	50°
i_d^0	0.5076 p.u.
i_q^0	0.8015 p.u.
e_d^0	0.2404 p.u.
e_q^0	0.9707 p.u.
E_q^0	1.1229 p.u.

Linearized constant values are given as shown in Table AIII.

TABLE AIII
LINEARIZED CONSTANT VALUES

Coefficient or parameter	Value
n_1	0.6744
n_2	0
m_1	0.8015
m_2	1.0526
K_1	0.7574
K_2	0.8015
K_3	0.3316
K_4	0.8615
K_5	1.1608
T_5	0.23 s
K_6	–0.1847
K_7	0.6641

REFERENCES

[1] A. Ulbig, T. S. Borsche, and G. Andersson, "Impact of low rotational inertia on power system stability and operation," *IFAC Proceedings*, vol. 47, no. 3, pp. 7290-7297, Aug. 2014.

[2] P. Kundur, *Power System Stability and Control*, 1st ed. New York: McGraw-Hill, 1994.

[3] U. Markovic, O. Stanojev, E. Vrettos *et al*., "Understanding small-signal stability of low-inertia systems," *IEEE Transactions on Power Systems*, doi: 10.1109/TPWRS.2021.3061434

[4] S. da Fonseca Santos, "Planning of power distribution systems with high penetration of renewable energy sources using stochastic optimization," Ph.D. dissertation, University of Beira Interior, Covilhã, Portugal, 2017.

[5] H. A. Alsiraji and R. El-Shatshat, "Comprehensive assessment of virtual synchronous machine based voltage source converter controllers," *IET Generation, Transmission & Distribution*, vol. 11, no. 7, pp. 1762-1769, May 2017.

[6] C. Sun, G. Joos, and F. Bouffard, "Identification of low-frequency oscillation mode and improved damping design for virtual synchronous machines in microgrid," *IET Generation, Transmission & Distribution*, vol. 13, no. 14, pp. 2993-3001, Jul. 2019.

[7] Q. C. Zhong and G. Weiss, "Synchronverters: inverters that mimic synchronous generators," *IEEE Transaction on Industrial Electronics*, vol. 58, no. 4, pp. 1259-1267, Apr. 2011.

[8] R. Aouini, B. Marinescu, K. B. Kilani *et al.*, "Synchronverter-based emulation and control of HVDC transmission," *IEEE Transactions on Power Systems*, vol. 31, no. 1, pp. 278-286, Jan. 2016.

[9] S. Dong and Y. C. Chen, "A method to directly compute synchronverter parameters for desired dynamic response," *IEEE Transactions on Energy Conversion*, vol. 33, no. 2, pp. 814-825, Jun. 2018.

[10] D. Chen, Y. Xu, and A. Q. Huang, "Integration of DC microgrids as virtual synchronous machines into the AC grid," *IEEE Transactions on Industrial Electronics*, vol. 64, no. 9, pp. 7455-7466, Sept. 2017.

[11] J. Fang, X. Li, and Y. Tang, "Grid-connected power converters with distributed virtual power system inertia," in *Proceedings of 2017 IEEE Energy Conversion Congress and Exposition (ECCE)*, Cincinnati, USA, Oct. 2017, pp. 4267-4273.

[12] M. Ndreko, S. Rüberg, and W. Winter, "Grid forming control for stable power systems with up to 100% inverter based generation: a paradigm scenario using the IEEE 118-bus system," in *Proceedings of 17th International Workshop on Large-scale Integration of Wind Power into Power Systems as well as on Transmission Networks for Offshore Wind Power Plants*, Stockholm, Sweden, Oct. 2018, pp. 1-6.

[13] P. Hu, H. Chen, K. Cao *et al.*, "Coordinated control of multiple virtual synchronous generators in mitigating power oscillation," *Energies*, vol. 11, no. 10, pp. 1-17, Oct. 2018.

[14] A. Ademola-Idowu and B. Zhang, "Optimal design of virtual inertia and damping coefficients for virtual synchronous machines," in *Proceedings of 2018 IEEE PES General Meeting (PESGM)*, Portland, USA, Aug. 2018, pp. 1-5.

[15] S. D'Arco , J. A. Suul, and O. B. Fosso, "Small-signal modelling and parametric sensitivity of a virtual synchronous machine," in *Proceedings of 2014 Power Systems Computation Conference*, Wroclaw, Poland, Aug. 2014, pp. 1-9.

[16] J. Liu, Y. Miura, and T. Ise, "Fixed-parameter damping methods of virtual synchronous generator control using state feedback," *IEEE Access*, vol. 7, pp. 99177-99190, Jul. 2019.

[17] J. Alipoor, Y. Miura, and T. Ise, "Power system stabilization using virtual synchronous generator with alternating moment of inertia," *IEEE Journal of Emerging and Selected Topics in Power Electronics*, vol. 3, no. 2, pp. 451-458, Jun. 2015.

[18] G. Bingtuan, X. Chaopeng, C. Ning *et al*., "Virtual synchronous generator based auxiliary damping control design for the power system with renewable generation," *Energies*, vol. 10, no. 8, p. 1146, Aug. 2017.

[19] G. Rogers, *Power System Oscillations*, 1st ed. Boston: Springer, 2000.

[20] E. Larsen and D. Swann, "Applying power system stabilizers, Part I: general concepts, Part II: performance objectives and tuning concepts, Part III: practical considerations," *IEEE Transactions on Power Apparatus and Systems*, vol. PAS-100, no. 6, pp. 3017-3024, Jun. 1981.

[21] P. W. Sauer, M. Pai, and J. H. Chow, *Power System Dynamic and Stability: with Synchrophasor Measurement and Power System Toolbox*, 2nd ed. New Jersey: Prentice Hall, John Wiley & Sons, 2018.

[22] B. Wang, N. Duan, and K. Sun, "A time-power series-based semi-analytical approach for power system simulation," *IEEE Transactions on Power Systems*, vol. 34, no. 2, pp. 841-851, Mar. 2019.

Karim Sebaa received the Electrical Engineering Degree and Magister in high voltage and power systems from Ecole Nationale Polytechnique, Algiers, Algeria, in 1998 and 2000, respectively. From September 2007 to March 2009, he was a visiting student at Suplélec French. Since 2003, He has joined the University of Medea, Medea, Algeria, where presently he is a Full Professor of power systems. His research interests include power system dynamics, distribution power system, and green energy integration into power system.

Yang Zhou received the B.Sc. degree from the College of Information Engineering, Xiangtan University, Xiangtan, China, in 2014, and the M.Sc. degree from the College of Electrical and Information Engineering, Hunan University, Changsha, China, in 2017. Since 2017, she has been working as a Research Associate at the Institute of Energy Systems, Energy Efficiency and Energy Economics, and she is currently pursuing the Ph.D. degree in electrical engineering at TU Dortmund University, Dortmund, Germany. Her current research interests include operation and control of hybrid AC/DC power system with energy storage systems for security and stability enhancement and flexibility of energy system.

Yong Li received the B.Sc. and Ph.D. degrees from the College of Electrical and Information Engineering, Hunan University, Changsha, China, in 2004 and 2011, respectively, and the second Ph.D. degree from TU Dortmund University, Dortmund, Germany, in 2012. He is currently a Full Professor of electrical engineering with Hunan University, Changsha, China. His research interests include power system stability analysis and control, AC/DC energy conversion systems and equipment, analysis and control of power quality, and HVDC and FACTS technologies.

Ayetül Gelen received the B.Sc. degree in electrical and electronics engineering from Kahramanmaraş Sütçü İmam University, Kahramanmaraş, Turkey, in 2003. She received the M.Sc. and Ph.D. degrees in electrical and

electronics engineering from Niğde University, Niğde, Turkey, in 2006 and 2012, respectively. She is currently working as an Assistant Professor in the Department of Electrical and Electronics Engineering of Bursa Technical University, Bursa, Turkey. Her research interests include power system modelling, alternative energy sources, distributed power systems and flexible AC transmission systems.

Hassan Nouri received the Ph. D. degree in electrical and electronic engineering from the University of Plymouth, Plymouth, UK. He is currently a Reader in electrical power and energy in the School of Engineering at the University of the West of England (UWE), Bristol, UK. He has over 25 years of involvement in academic life with experience of research and departmental teaching in UK Universities. He was Chairman of the European Electromagnetic User Group (EEUG) from 2004 to 2010 and he has served on numerous editorial boards for Electrical Power Engineering Journals. Over the years, his research has been funded by the Engineering and Physical Sciences Research Council (UK), the European Union, the Royal Society (UK), the British Council (UK), and the Power Industry (UK, Germany and Korea). In 2004, he was awarded the IEEE PES Chapter outstanding Engineer award in recognition of his service in power engineering research and to the UKRI Chapter. His research interests include power system analysis, power electronics application, electric arc modeling, fault location and power quality.